PHYSICS OF TISSUES AS ACTIVE FLUIDS

G. SALBREUX

1. Introduction

We will discuss here the physical behaviour of tissues on large scales much larger than a cell size. Morphogenetic motion during embryonic development relies on the collective motion of thousands of cells that deform to establish the shape of the organism. At the scale of an organ, we expect emergent features to appear that are independent of many details of the cellular organisation. The question here is how the principle of "more is different" (P.W. Anderson, Science, 1977) is realised in biology going from a single cell to an entire tissue.

1.1. **Tissue organisation.**

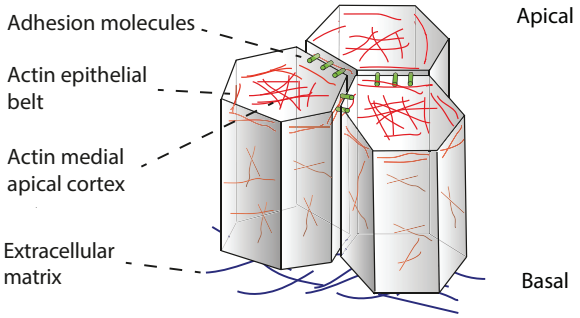

We briefly summarize key aspects of the organization of cells in epithelia. Epithelial cells have an apico-basal polarity with different sets of proteins and cellular structures present in the apical and basal regions. The basal cellular interfaces adhere to an external polymer network, the extracellular matrix, through specific structures such as focal adhesions. Cells adhere to each other through adhesion molecules, such as cadherins, which go across the cell membrane. On the intracellular side, cadherins are bound, indirectly, to an actomyosin network. The actomyosin cytoskeleton is a cellular structure made of actin filaments and myosin molecular motors which are strongly concentrated near the cell membrane. Within this actin polymer network, myosin molecular motors exert internal tensions, which allow cells and tissues to deform.

In the following we will discuss a two-dimensional description of flat epithelia. The idea is that three-dimensional aspects of tissue mechanics are effectively captured by two-dimensional parameters. We use the cartesian basis $\mathbf{e}_x$, $\mathbf{e}_y$ and denote by latin indices $i, j, ...$ the space coordinates x, y.

1.2. **Rheology.** To discuss the mechanical response of a tissue, we introduce some notions of rheology. Rheology describes how materials can flow. A Newtonian fluid has a particularly simple rheology and obeys the constitutive equation

$$\tilde{\sigma}_{ij} = 2\eta \tilde{v}_{ij} \tag{1}$$

where $\tilde{\sigma}_{ij}$ is the traceless part of the symmetrized stress tensor, η the viscosity and $\tilde{v}_{ij}$ is the anisotropic part of the gradient of flow (see section 3.1 for a precise definition). In this simple case, a gradient of flow is creating a stress, which vanishes when the flow stops, and one postulates a linear relation between a thermodynamic flux (the gradient of flow) and a thermodynamic force (the stress tensor).

To discuss more complex rheology, we consider here simple 1D systems. In the one-dimensional case, a viscous element with a Newtonian fluid law would have the constitutive equation

$$f = \mu \frac{dx}{dt} \tag{2}$$

with μ the viscosity of the viscous element, x the deformation, and f the force acting on the element. Such an element is called a dashpot. A spring element, by contrast, is an elastic element and has constitutive equation

$$f = kx \tag{3}$$

with k a spring modulus. By contrast to a viscous element, an elastic element can sustain a stress at constant deformation x.

"Rheological schemes" describe more complex behaviour occurring on different timescales, and are obtained by combining different basic rheological elements. Two examples are shown below for the Maxwell (left) and Kelvin-Voigt (right) rheology which are two simplified descriptions of a viscoelastic material.

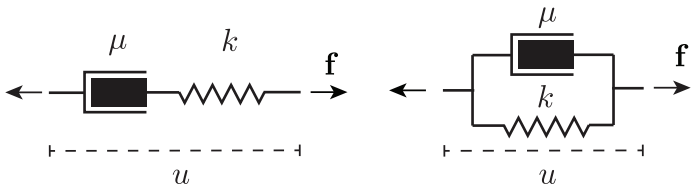

A material with a Maxwell rheology is fluid on long time scales, while a material with a Kelvin-Voigt rheology is elastic on long time scales. The Maxwell element is made of a dashpot (with viscosity μ) and a spring (with elastic modulus k) in series, while the Kelvin-Voigt element is made of a dashport and a spring in parallel. Considering the total deformation and total force in each of these systems, one can see that the force f and deformation u are related to each other by

$$\left(1 + \tau \frac{d}{dt}\right) f = \mu \frac{du}{dt} \qquad \text{Maxwell}, \tag{4}$$

$$\frac{df}{dt} = k \left(1 + \tau \frac{d}{dt}\right) \frac{du}{dt} \qquad \text{Kelvin} - \text{Voigt}, \tag{5}$$

where $\tau = \frac{\mu}{k}$ is a characteristic time scale that can be constructed from the ratio of the dashpot viscosity and the spring elastic modulus. In each case the long time behaviour can be found by setting the limit $\frac{d}{dt} \to 0$; one can see then that on long time scale the Maxwell element has constitutive equation $f = \mu du/dt$ (a purely viscous behaviour); while the Kelvin-Voigt element has constitutive equation $f \sim ku$ (a purely elastic behaviour).

2. Broken symmetries: tissues as living liquid crystals

Cells are not isotropic objects: they can have a preferred axis of elongation, or establish an anisotropic cellular organization. On large scales, tissues can therefore be seen as collections of individual anisotropic objects. This feature is reminiscent of liquid crystals which are made of (much simpler) anisotropic molecules. We therefore expect some aspects of the physics of liquid crystals to appear in tissues.

2.1. **Cell polarity.**

2.1.1. *Cell polarization.* Cells can spontaneously polarize themselves by segregating proteins at opposite ends of the cell. This is thought to be achieved by proteins which bind to the cell membrane, or to the cell actomyosin cortex at the cell membrane, but also repress each other (i.e., negatively affect the binding affinity of other proteins). This can ensure that two different types of proteins tend to accumulate in different regions of the cell. For instance, epithelial tissues have a main apico-basal axis that distinguishes the "top" and "bottom" of the nearly two-dimensional epithelial surface. In addition, planar-cell polarity proteins establish a preferred cell direction in the plane of the tissue, orthogonal to the apico-basal axis. To capture the main axis of organization of polarity proteins, a polarity vector $\mathbf{p}$ can be associated to a cell, based on the first moment in the distribution of polarity proteins. For instance, we denote here $A(\theta)$ and $B(\theta)$ the normalized concentrations of two polarity proteins A and B along the contour of a 2D section of a cell. A point on the contour is labelled by the angle θ measured to the center of the cell. The concentrations are normalized such that $\int_0^{2\pi} d\theta A(\theta) = 1$, and similarly for B. One can define a polarity vector through

$$\mathbf{p} = \begin{pmatrix} \int_0^{2\pi} d\theta (A(\theta) - B(\theta)) \cos\theta \\ \int_0^{2\pi} d\theta (A(\theta) - B(\theta)) \sin\theta \end{pmatrix} . \tag{6}$$

One can verify that with this definition, if A and B are both uniformly distributed, then $\mathbf{p} = 0$. If A and B are not uniform, the vector $\mathbf{p}$ points towards A-rich regions, away from B rich regions.

2.1.2. *A simple model for C. elegans embryo polarization.*

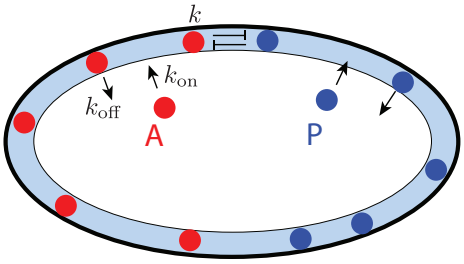

A model system studied to understand cell polarization is the early anterio-posterior polarization of the *C. elegans* embryo. During this biological process, a symmetry-breaking event occurs, establishing the first antero-posterior axis of the animal. A set of polarity proteins segregate at the anterior and posterior cell ends. A model proposed to understand the establishment of polarization reads

$$\partial_t A = D\partial_x^2 A + k_{\rm on} - \left[k_{\rm off} + kP^2\right] A \tag{7}$$

$$\partial_t P = D\partial_x^2 P + k_{\rm on} - \left[k_{\rm off} + kA^2\right] P \tag{8}$$

where A and P are the surface concentrations of an anterior and posterior marking protein. The diffusion constant of polarity protein at the cell surface D and their on-rate $k_{\rm on}$ are taken to be identical for A and P for simplicity. The on-rate $k_{\rm on}$ also absorbs the cytoplasmic concentration which is assumed to be constant. The off rate of each protein is modulated by the concentration of the other protein, reflecting interactions between the two proteins. The terms in k have exponents in A and P which reflect molecular mechanisms contributing to the unbinding event; here one has assumed that a complex formed of two molecules of one type is necessary to promote the unbinding of the other type.

To study this system of equations, it is easier to reduce the number of parameter by normalizing time ($\bar{t} = tk_{\rm off}$) and concentrations ($\bar{A} = A/(k_{\rm on}/k_{\rm off})$, $\bar{P} = P/(k_{\rm on}/k_{\rm off})$), which leads to:

$$\begin{aligned}\partial_{\bar{t}}\bar{A} &= \ell^2\partial_x^2\bar{A} + 1 - \left[1 + \bar{k}\bar{P}^2\right]\bar{A}\\ \partial_{\bar{t}}\bar{P} &= \ell^2\partial_x^2\bar{P} + 1 - \left[1 + \bar{k}\bar{A}^2\right]\bar{P}\ ,\end{aligned} \tag{9}$$

where $\ell = \sqrt{D/k_{\rm off}}$ is a characteristic length of diffusion and $\bar{k} = kk_{\rm on}^2/k_{\rm off}^3$ is an adimensional coefficient.

It is then instructive to look for homogeneous solutions ($\partial_x^2\bar{A} = 0$ and $\partial_x^2\bar{P} = 0$) and plot the nullclines (the lines in the space $(\bar{A}, \bar{P})$ for which $\partial_t\bar{A} = 0$ and $\partial_t\bar{P} = 0$). The nullclines equations are $\bar{P} = \sqrt{\frac{1}{k}\left(\frac{1}{\bar{A}} - 1\right)}$ and $\bar{P} = \frac{1}{1+\bar{k}\bar{A}^2}$ and are plotted below for two different values of $\bar{k}$.

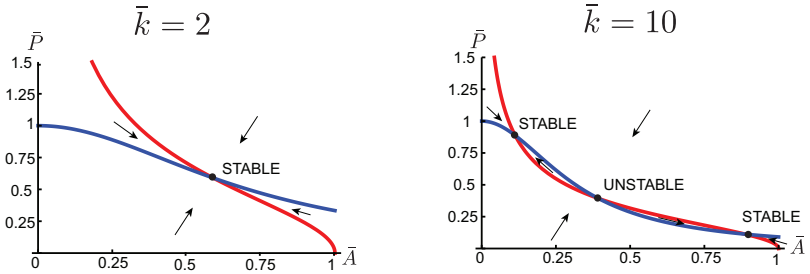

The nullclines intersect at possible homogeneous solutions for A and P. The arrows indicate schematically the direction of the vector $(\partial_t \bar{A}, \partial_t \bar{P})$, allowing to visually guess the stable and unstable solutions. For $\bar{k} < 4$ one stable homogeneous solution exists, for $\bar{k} > 4$ two stable solutions and one unstable solution appear.

The appearance of bistability allows the system to support regions with a high (respectively low) concentration of A and low (respectively high) concentration of P. The plots below show steady-state solutions of Eq. 9 on a domain $0 < x < L$ with no flux boundary conditions, $\partial_x A|_{x=0} = \partial_x A_{x=L} = \partial_x P|_{x=0} = \partial_x P|_{x=L} = 0$. Depending on the initial condition, the system can reach a A or P high state, or a coexistence state where an interface appears between A-rich and P-rich domains. In this last polarized cell state, the width of the interface is related to the diffusion-associated length ℓ.

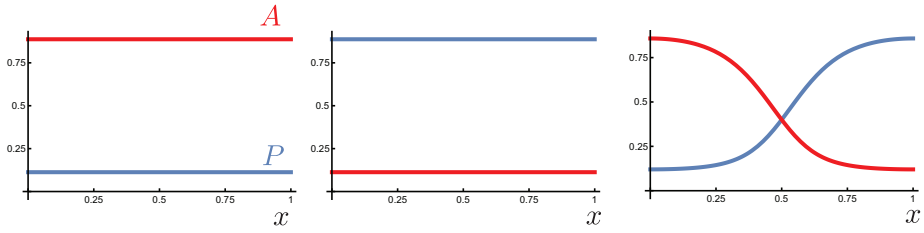

2.1.3. *Planar polarity patterns.* In an epithelium, cells can spontaneously polarize in the plane, choosing an orientation which is consistent between neighbouring cells. This is achieved by interactions between polarity proteins across cellular interfaces.

On scales much larger than the cells, the tendency of cell neighbours planar-cell polarity to align with each other give rise to large-scale polarity patterns. In analogy with a passive liquid-crystal, one expects an effective energetic cost to be associated with non-zero gradients of polarity, which can be written

$$F = \int_{\mathcal{S}} dS \frac{K}{2} (\partial_i \mathbf{p})^2 + \int_{\mathcal{S}} dS \lambda (\mathbf{p}^2 - 1) \ , \tag{10}$$

where K is called the Frank constant and the first term in F is the Frank free energy. The constant K penalizes distorsions in the polarity field $\mathbf{p}$. The second term in F involves a Lagrange multiplier λ which enforces that $\mathbf{p} = 1$. One can then define $\mathbf{h}$ the molecular field:

$$\mathbf{h} = -\frac{\delta F}{\delta \mathbf{p}} = K \Delta \mathbf{p} - 2\lambda \mathbf{p}$$

where Δ is the Laplacian operator. $\mathbf{h}$ can be seen as the driving force arising from the system effective free energy, which tends to make the polarity field rotate. At equilibrium, the effective free energy is minimized and $\mathbf{h} = 0$.

A striking example of such polar patterns can be seen in the *Drosophila* pupal wing. During pupal wing development, the tissue elongates along the proximal-distal direction (horizontal axis in the schematic below). At the same time, the planar polarity reorients to align with the elongation axis of the wing:

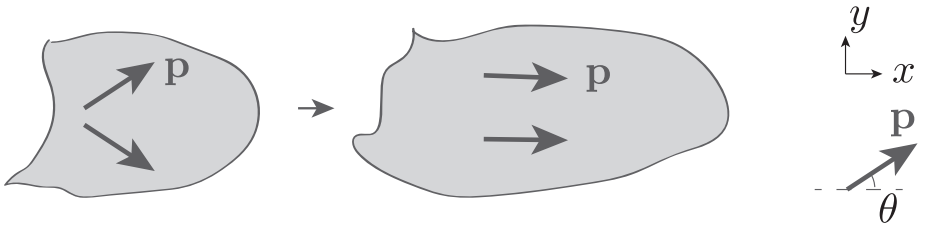

We now discuss this process using a continuum theory of polar fluids. We write a linear phenomenological equation for the evolution of the polarity field, which is inspired by the physics of liquid crystals:

$$\frac{Dp_i}{Dt} = \frac{1}{\gamma_1} h_i - \nu p_j \tilde{v}_{ij} \ , \tag{11}$$

where the corotational time derivative reads

$$\frac{Dp_i}{Dt} = \frac{\partial p_i}{\partial t} + v_j \partial_j p_i + w_{ij} p_j \tag{12}$$

with $\omega_{ij} = \frac{1}{2}(\partial_i v_j - \partial_j v_i)$ is associated to the rotational curl of the velocity field. The first term in Eq. 12 is the actual time variation of the polarity, the second term correspond to advection of polarity by the flow, the third term to rotation of the polarity by the flow. In Eq. 11, the first term describes the relaxation due to the molecular field, and γ_1 is a rotational viscosity. The second term is a flow-alignment term that arises from the fact that the polarity can reorient under a shear flow, with ν a phenomenological coefficient. The traceless symmetric part of the flow gradient, $\tilde{v}_{ij}$, is defined in section 3.1. We consider here a case where $\nu < 0$. In the absence of flow, Eq. 11 describes a dynamic relaxation to the equilibrium state, characterized by $\mathbf{h} = 0$.

For simplicity we assume that the order parameter is homogeneous in space. In that case the free energy of the system (Eq. 10) reduces to $F_0 = \int_S dS \lambda(\mathbf{p}^2 - 1)$, and the molecular field is then given by $\mathbf{h} = -2\lambda \mathbf{p}$. The Lagrange multiplier can be determined by imposing $p_i \frac{\partial p_i}{\partial t} = 0$, a consequence of $\mathbf{p} = 1$. One then obtains from Eq. 11:

$$\begin{aligned} p_i \omega_{ij} p_j &= -\frac{1}{\gamma_1} p_i 2\lambda p_i - \nu p_j p_i \tilde{v}_{ij}, \\ \lambda &= -\frac{\gamma_1}{2} p_i p_j (\omega_{ij} + \nu \tilde{v}_{ij}) \ . \end{aligned} \tag{13}$$

The uniform polar field in 2D is now written $\mathbf{p} = (\cos\theta, \sin\theta)$. The deformation of the tissue is represented by an elongational flow $v_x = k_e x$, where k_e is the rate of tissue

elongation. We then obtain a dynamic equation for the angle θ in this flow:

$$\begin{aligned} \frac{dp_x}{dt} &= p_x \nu \frac{k_e}{2}\left(p_x^2 - p_y^2\right) - \nu p_x \frac{k_e}{2} \\ -\sin\theta \frac{d\theta}{dt} &= -\cos\theta \frac{\nu}{2} k_e (1 - \cos^2\theta + \sin^2\theta) \\ \frac{d\theta}{dt} &= \frac{\nu k_e}{2}\sin(2\theta) \end{aligned} \tag{14}$$

One can see from this equation that the possible stationary solutions for the polarity orientation under the flow are $\theta = k\pi/2$ with k an integer. In the interval $0 \leqslant \theta < 2\pi$, only the solution $\theta = 0$ and $\theta = \pi$ are actually stable. The stability of the solution $\theta = 0$ can been seen by expanding the dynamic equation 14, for small $\theta << 1$:

$$\frac{d\theta}{dt} \simeq \nu k_e \theta$$

and the angle θ has solution

$$\theta = \theta_0 e^{\nu k_e t}$$

which relaxes exponentially to $\theta = 0$ for $\nu < 0$, with a time scale $\tau = 1/(-\nu k_e)$. This also means that if the system starts with an angle $\theta_0 \neq 0$ sufficiently small, the polarity will reorient towards the elongation axis ($\theta = 0$) as the tissue elongates.

Returning to the biological system, this analysis shows that the elongation of a tissue during morphogenesis can in principle drive an alignment of the cells planar polarity axis, along the axis of tissue elongation.

2.2. **Cell elongation.** We now turn to cell elongation. When looking at the apical surface of an epithelium, it is clear that cell shapes are not isotropic, i.e. are not generally circular. We then seek to characterize cell shape by a simple quantification. One could in principle associate a polarity field to the shape by defining a vector $\mathbf{p}_S$:

$$\mathbf{p}_S = \frac{1}{2\pi R}\begin{pmatrix} \int_0^{2\pi} d\theta r(\theta)\cos\theta \\ \int_0^{2\pi} d\theta r(\theta)\sin\theta \end{pmatrix}, \tag{15}$$

where $r(\theta)$ denotes the position of the contour of the cell at angle θ, in polar coordinates away from the cell center, and we also have introduced $R = \frac{1}{2\pi}\int_0^{2\pi} d\theta r(\theta)$ the average radius. It turns out however that in a typical epithelium the cell shape is better characterized by the next order nematic order parameter:

$$\mathbf{Q}^{\text{cell}} = \begin{pmatrix} Q_{xx}^{\text{cell}} & Q_{xy}^{\text{cell}} \\ Q_{xy}^{\text{cell}} & Q_{yy}^{\text{cell}} \end{pmatrix} = \frac{1}{2\pi R}\begin{pmatrix} \int_0^{2\pi} d\theta r(\theta)\cos 2\theta & \int_0^{2\pi} d\theta r(\theta)\sin 2\theta \\ \int_0^{2\pi} d\theta r(\theta)\sin 2\theta & -\int_0^{2\pi} d\theta r(\theta)\cos 2\theta \end{pmatrix} \tag{16}$$

which quantifies cell elongation. The tensor $\mathbf{Q}^{\text{cell}}$ is symmetric and traceless, therefore it has only two independent components. Rewriting the nematic tensor $\mathbf{Q}^{\text{cell}}$ as

$$\mathbf{Q}^{\text{cell}} = 2S\begin{pmatrix} n_x^2 - \frac{1}{2} & n_x n_y \\ n_x n_y & n_y^2 - \frac{1}{2} \end{pmatrix}, \tag{17}$$

defines the strength of cell elongation, $S = \sqrt{(Q_{xx}^{\text{cell}})^2 + (Q_{xy}^{\text{cell}})^2}$, and a normalized nematic vector $\mathbf{n}$ which verifies $\mathbf{n}^2 = 1$ and gives the axis of cell elongation. Both $\mathbf{n}$ and $-\mathbf{n}$ correspond to the same tensor $\mathbf{Q}$, as required by the fact that the nematic order parameter does not vary by rotation of π of the elements of the system.

Once a cell elongation axis $\mathbf{n}$ has been associated to cells in the tissue, a large-scale average cell elongation tensor can be defined from:

$$Q_{ij} = \langle Q_{ij}^{\text{cell}} \rangle \ , \tag{18}$$

where the averaging operator has a possible definition for a quantity f_α which varies between cells labelled α,

$$\langle f \rangle = \frac{\sum_{\text{cell } \alpha} A_\alpha f_\alpha}{\sum_{\text{cell } \alpha} A_\alpha} \ . \tag{19}$$

This definition has the advantage of giving a smaller weight in the averaging to cells that occupy a smaller area of the tissue.

2.3. **Nematostatics.** When culturing *in vitro* elongated cells, it is found for some cell types that large-scale nematic structures emerge where neighboring cells tend to align their axis of cell elongation. This is reminiscent of the planar polarity patterns discussed in section 2.1.3. As in the case of planar polarity, one expects that the tendency of the system to eliminate spatial distorsion of the nematic axis can be captured by minimization of the effective Frank free energy:

$$F = \int dS \frac{K}{2} (\partial_i \mathbf{n})^2 \ . \tag{20}$$

Below we consider a situation where $\mathbf{n} = 1$ and one denotes the angle ϕ such that $\mathbf{n} = (\cos\phi, \sin\phi)$. The angles ϕ and $\phi + \pi$ refer to the same nematic state. In that case the distorsion effective free energy can be rewritten $F = \int dS \frac{K}{2} (\partial_i \phi)^2$; minimizing the energy with respect to ϕ yields the equation

$$\Delta \phi = 0 \tag{21}$$

with $\Delta = \partial_x^2 + \partial_y^2$ the Laplacian operator.

Cellular elongation patterns, as orientation patterns seen in nematic liquid crystals, can exhibit point defects. A defect is a point where the nematic angle is not defined. Defects can be classified according to their topological charges. The "topological charge" enclosed within a curve $\mathcal{C}$ is defined by

$$m = \frac{1}{2\pi} \oint_{\mathcal{C}} dl_i \partial_i \phi \ , \tag{22}$$

where the integral is taken on the curve $\mathcal{C}$, and has positive orientation (see below for an example of such a curve). $\mathbf{dl}$ is an infinitesimal displacement along the curve.

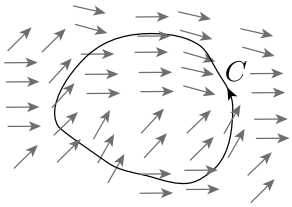

The topological charge quantifies how much the vector field rotates along the curve: one full rotation in the clockwise direction contributes a charge 1, one full rotation in the anticlockwise direction a charge -1. Importantly, the topological charge around a defect does not depend on the precise shape of the enclosing curve $\mathcal{C}$.

To find the nematic profile around a defect, one can note that in polar coordinates the Laplacian operator reads $\Delta = \partial_r^2 + \frac{1}{r}\partial_r + \frac{1}{r^2}\partial_\theta^2$. Looking for a solution of Eq. 21 that does not depend on r, one is led to

$$\phi(r,\theta) = m\theta + a \tag{23}$$

where m is the nematic charge of the defect as can be seen by application of Eq. 22. For a nematic defect, m must be a multiple of $1/2$ to ensure proper periodicity as θ goes from 0 to 2π (for a nematic ϕ and $\phi+\pi$ are equivalent). Changing the constant a leads to an overall solid rotation of the pattern of the defect. The associated distorsion energy of a defect of charge m is, by application of Eq. 20, $F_m = \pi K m^2 \log \frac{R}{r_c}$, where R and r_c are an upper and lower cut-off lengths around the defect (in the core of the defect the assumption $\mathbf{n} = 1$ must break down). From this relation, one sees that defects with a smaller topological charge have a lower effective energy and are more favourable.

Below are shown the corresponding solutions for the lowest-charge defects $m = \frac{1}{2}$ and $m = -\frac{1}{2}$:

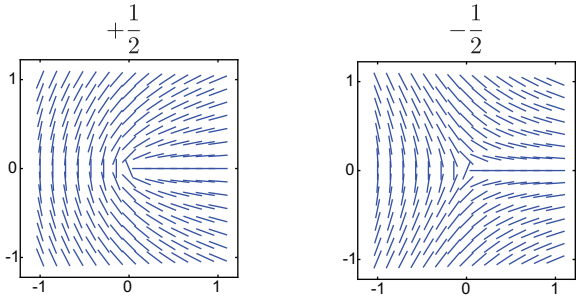

One can note that the two $\pm\frac{1}{2}$ defects have themselves different symmetries: the $+\frac{1}{2}$ defect has a preferred direction (left to right above), while the $-\frac{1}{2}$ defect has a 3-fold rotational symmetry. As a result, in an active system, the $+\frac{1}{2}$ system can acquire a spontaneously velocity, but the $-\frac{1}{2}$ defect can not.

We now discuss experimental results observing patterns of an elongated cell type cultured *in vitro* (NIH 3T3 mouse embryo fibroblasts). The tissue is grown on a circular disc. Cells tend to orient their axis of elongation parallel to the external interface, a very general observation in tissues *in vivo* and *in vitro*. On a disc this enforces a total topological

charge of 1; therefore defects must arise within the tissue. The number of visible nematic defects decrease over time as the tissue dynamically rearranges and defects of opposite charge annihilate. Eventually the system converges to an organization with only two $+\frac{1}{2}$ defects which form at a reliable position within the disc. This is consistent with effective energy arguments described above - the system prefers to choose defect with low charges. One can in fact go further and show that the final position of defects is also predicted by minimizing the effective distorsion energy introduced above. This is a beautiful example of the fact that on large scale, it can happen that many of the details of cellular organization do not matter, and the tissue-scale behaviour can be predicted by simple generic physical arguments.

3. Shear decomposition

We now discuss tissue shear, i.e. the dynamics of tissue deformation. The fundamental question in this section is how to relate cell and tissue deformation.

3.1. **Isotropic and anisotropic shear.**

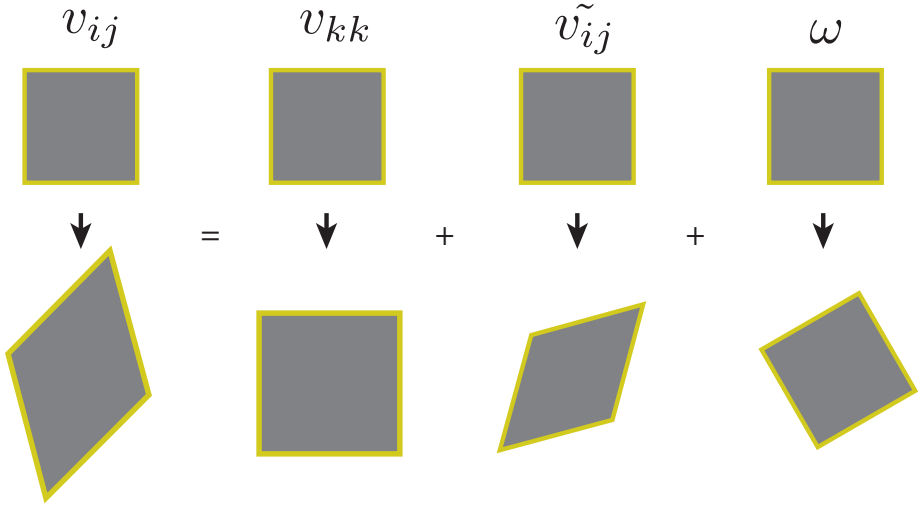

We denote $\mathbf{v}$ the velocity field in the tissue. Deformations can be quantified by considering spatial gradient of the velocity field. The velocity gradient tensor $v_{ij} = \partial_i v_j$ can be decomposed into three basic components

$$v_{ij} = \frac{1}{2}\underbrace{v_{kk}\delta_{ij}}_{\text{isotropic}} + \underbrace{\tilde{v}_{ij}}_{\text{anisotropic, area-preserving}} + \underbrace{\omega\epsilon_{ij}}_{\text{rotation}}, \tag{24}$$

where $v_{kk} = v_{xx} + v_{yy}$ is the trace of the velocity gradient, and describes isotropic contraction or expansion, corresponding to changes of tissue area. We refer to it as the "isotropic shear". The second term in the decomposition, $\tilde{v}_{ij} = \frac{1}{2}(v_{ij} + v_{ji}) - \frac{v_{kk}}{2}\delta_{ij}$ is the traceless symmetric part of the velocity gradient and describes pure shear (i.e. anisotropic deformation which preserves the area). This is the "anisotropic shear". The

antisymmetric part of the velocity gradient describes local rotations and can also be written $\omega_{ij} = \omega\epsilon_{ij} = \frac{1}{2}(\partial_i v_j - \partial_j v_i)$. Here, ϵ_{ij} is defined as the antisymmetric tensor with $\epsilon_{xx} = \epsilon_{yy} = 0$, $\epsilon_{xy} = 1$ and $\epsilon_{yx} = -1$. $\omega = \frac{1}{2}v_{ij}\epsilon_{ij}$ is the rotational curl of the velocity field. This decomposition is a mathematical identity and is therefore exact. Local solid rotations described by ω_{ij} do not correspond to local material deformations, so in the following we focus on the isotropic and anisotropic shear.

Below we discuss cellular contributions to the isotropic and anisotropic shear.

3.2. **Isotropic shear decomposition.** The isotropic shear decomposition essentially arises from the balance of number of cells. This equation can be written

$$\partial_t n + \partial_i(n v_i) = n(k_d - k_a) \tag{25}$$

where n is the cell number density (number of cells per unit area), $n\mathbf{v}$ is the cell flux, quantifying the transport of cells by the flow, k_d is the rate of cell division, and k_a the rate of cell apoptosis (or delamination from an epithelium). This balance equation follows the generic form, for a quantity f,

$$\partial_t f + \partial_i j_i^f = s^f \tag{26}$$

where $\mathbf{j}^f$ is a flux, describing spatial redistribution of the quantity f and s^f is a source term, describing destruction and creation of f. Accordingly in Eq. 25, in the absence of cell division and death, the cell number density n is a conserved quantity (i.e., in a closed system with no flow at the boundary, $\partial_t(\int dS n) = 0$) and only locally changes according to the flux $\mathbf{j}^n = n\mathbf{v}$. The term in the right-hand-side of Eq. 25, $n(k_d - k_a)$ is a source term that describes creation and destruction of cells.

Eq. 25 can be written in a slightly different form, which makes the isotropic shear decomposition more transparent:

$$v_{kk} = \partial_k v_k = \frac{1}{a}\frac{Da}{Dt} + k_d - k_a \tag{27}$$

where $a = 1/n$ is the average cell area, and $Da/Dt = \partial_t a + v_i \partial_i a$ is the convected time derivative of the average cell area. Under this form, we see that the tissue flow divergence (or relative rate of area change) arises either from a change in the average cell area, or through creation or destruction of cells through cell division or apoptosis.

3.3. **Anisotropic shear decomposition.** Anisotropic shear can also be decomposed into fundamental contributions. Intuitively, we expect that tissue shear can stem from cellular deformation, simply because if every cell elongates in a tissue, the tissue elongates as well. Cell elongation can be quantified by a nematic tensor Q_{ij}, as described in section 2.2. The relationship between tissue shear and cell elongation change can then be written

$$\tilde{v}_{ij} = \frac{DQ_{ij}}{Dt} \tag{28}$$

with D/Dt the corotational derivative:

$$\frac{DQ_{ij}}{Dt} = \partial_t Q_{ij} + v_k \partial_k Q_{ij} + \omega_{ik} Q_{kj} + \omega_{jk} Q_{ki} \ . \tag{29}$$

In Eq. 28, the anisotropic shear $\tilde{v}_{ij}$ is a deformation per unit time, and the right hand side is the time derivative of a measure of cell elongation, so that the relation is dimensionally consistent.

However, Eq. 28 does not capture all possible sources of deformation in a tissue. This is because cells can not only elongate, but also undergo events of cell division, cell delamination (when a cell disappears from the tissue), and cell neighbour exchange. A schematic for these three different events is shown below.

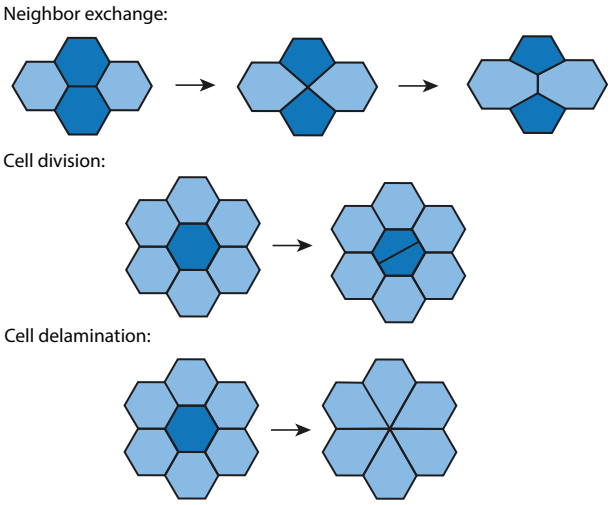

All these events can contribute to tissue deformation, without change in cell shape; or alternatively can lead to cell deformation without the boundary of the tissue moving. As a result a more general shear decomposition can be written as

$$\tilde{v}_{ij} = \frac{DQ_{ij}}{Dt} + R_{ij} \tag{30}$$

where R_{ij} is a tensor of cellular rearrangements.

We now describe a method to calculate these contributions to tissue anisotropic deformation, from observations of a deforming 2D tissue. We assume that we have measurements of the cells positions and topology at times $t_n = 0, \Delta t, ...n\Delta t, ...$ The idea is to decompose the tissue deformation occurring between t_n and t_{n+1} into several steps. So denoting O_n the state of the tissue at time t_n, one constructs the intermediate artificial states I_n^1, I_n^2, I_n^3 between O_n and O_{n+1}, as follows:

$$O_n \xrightarrow{\text{delamination}} I_n^1 \xrightarrow{\text{pure deformation}} I_n^2 \xrightarrow{\text{neighbour exchange}} I_n^3 \xrightarrow{\text{divisions}} O_{n+1} \ . \tag{31}$$

Here I_n^3 is constructed from O_{n+1} by "undoing" cell divisions. I_n^1 is constructed from O_n by removing all cells that will undergo a delamination between t_n and t_{n+1} (but keeping otherwise the tissue state as in O_n). I_n^2 is obtained by displacing the cell centers in I_n^1 to have the position they reach in I_n^3. What is left between I_n^2 and I_n^3 are then cellular neighbour exchange events, but which occur at fixed cell center positions.

From this set of decomposition, the change in average tissue cell elongation between O_n and O_{n+1} can then be written

$$\begin{aligned}\underbrace{\langle Q_{ij}(O_{n+1})\rangle - \langle Q_{ij}(O_n)\rangle}_{\text{cell elongation}} &= \underbrace{\left[\langle Q_{ij}(I_n^1)\rangle - \langle Q_{ij}(O_n)\rangle\right]}_{\text{delaminations}} + \underbrace{\left[\langle Q_{ij}(I_n^2)\rangle - \langle Q_{ij}(I_n^1)\rangle\right]}_{\text{cell center motion}} \\ &+ \underbrace{\left[\langle Q_{ij}(I_n^3)\rangle - \langle Q_{ij}(I_n^2)\rangle\right]}_{\text{neighbour exchange}} + \underbrace{\left[\langle Q_{ij}(O_{n+1})\rangle - \langle Q_{ij}(I_n^3)\rangle\right]}_{\text{divisions}}\end{aligned} \tag{32}$$

If we divide each side of this relation by Δt, we see that we are close to a relation of the form of Equation 30, rewritten as $\frac{DQ_{ij}}{Dt} = \tilde{v}_{ij} - R_{ij}$. Indeed, the left-hand side is a change of cell elongation, and the right hand side contains changes due to various cellular rearrangements. The contribution due to "cell center motion" is close to what expect will correspond to the anisotropic tissue shear $\tilde{v}_{ij}$.

To make this contribution more clear, we use a specific way to calculate cell elongation which is convenient for the decomposition above. We define a dual network of triangles which is obtained by connecting the cell centers of nearest neighbours. Instead of calculating elongation cell by cell, the tissue elongation is then calculated by taking the average triangle elongation in the dual network. With this definition, a cellular rearrangement is associated to a swap in how a quadrilateral can be divided into two triangles, as in the example below:

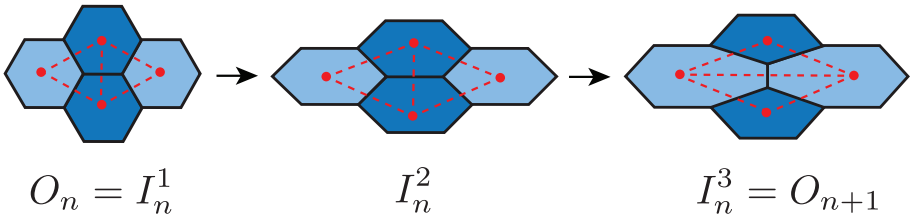

This swap event is at the origin of the shear by cellular rearrangement in the shear decomposition method.

To relate the change in triangle elongation coming from "cell center motion" to the shear, one starts with the observation that the shear associated to a triangle with vertices $\mathbf{x}^1$, $\mathbf{x}^2$, $\mathbf{x}^3$ and associated velocities $\mathbf{v}^1$, $\mathbf{v}^2$, $\mathbf{v}^3$ can be uniquely defined by the set of equations

$$\begin{aligned} v_i^2 - v_i^1 &= v_{ji}(x_j^2 - x_j^1) \\ v_i^3 - v_i^1 &= v_{ji}(x_j^3 - x_j^1)\ . \end{aligned} \tag{33}$$

In the equations above, there are 4 equations (since $i = x, y$) and 4 unknowns, the components of v_{ij}.

On the other hand, the elongation of a triangle can be defined uniquely by comparing the triangle with an equilateral triangle, with an horizontal base and an arbitrary side length. This comparison defines an affine transformation s_{ij}, which can be obtained from

the set of equations

$$\begin{aligned} x_i^2 - x_i^1 &= s_{ij}(e_j^2 - e_j^1) \\ x_i^3 - x_i^1 &= s_{ij}(e_j^3 - e_j^1) \ , \end{aligned} \tag{34}$$

where $\mathbf{e}^\alpha$ are the vertices of the reference triangle. The triangle elongation can then be defined by decomposing uniquely $\mathbf{s}$ into a rotation $\mathbf{r}$, a pure shear transformation $e^{\mathbf{Q}}$ parameterized by a traceless symmetric elongation tensor $\mathbf{Q}$, and an area change:

$$\mathbf{s} = \sqrt{\frac{a}{a_0}} e^{\mathbf{Q}} \cdot \mathbf{r} \ , \tag{35}$$

where a_0 is the area of the reference triangle. Mathematically this relation arises from a matrix polar decomposition of $\mathbf{s}$.

This now defines the elongation tensor for a triangle $\mathbf{Q}$, which can be plugged in Eq. 32. As shown in the schematic below, one then wishes to relate the change of triangle shape, quantified by $\mathbf{s}$, to the shear, quantified by v_{ij}.

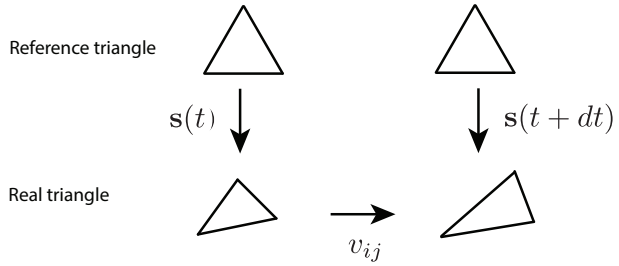

Combining Eqs. 33 and 34 above, one can verify that

$$\frac{ds_{ij}}{dt} = v_{ki} s_{kj} \ . \tag{36}$$

Then combining Eq. 35 and 36, one can verify [1] that for a single triangle, and for small triangle elongation $|\mathbf{Q}| \ll 1$,

$$\tilde{v}_{ij} \simeq \frac{dQ_{ij}}{dt} + 2\omega_{ik} Q_{kj} \ . \tag{39}$$

One can see in this relation that the triangle shear is not purely its change of elongation, but also involves a corotational term. Using this expression to replace $\langle Q_{ij}(I_n^2)\rangle - \langle Q_{ij}(I_n^1)\rangle$

[1] This can be proven as follows for small elongation $|\mathbf{Q}| \ll 1$. One has $e^{\mathbf{Q}} \simeq \mathbf{1} + \mathbf{Q}$ and $s_{ij} \simeq \sqrt{\frac{a}{a_0}}(r_{ij} + Q_{ik} r_{kj})$. Using that $\mathbf{r}$ is a rotation and denoting θ its angle, $\frac{dr_{kj}}{dt} = -\frac{d\theta}{dt} r_{kl}\epsilon_{lj}$. Then taking the time derivative of Eq. 35, one has

$$\frac{ds_{ij}}{dt} \simeq \frac{1}{2a}\frac{da}{dt} s_{ij} + \frac{dQ_{ik}}{dt} s_{kj} - \frac{d\theta}{dt} s_{ik}\epsilon_{kj} \tag{37}$$

$$\simeq \left[\frac{1}{2a}\frac{da}{dt}\delta_{ik} + \frac{dQ_{ik}}{dt} - \frac{d\theta}{dt} s_{il}\epsilon_{lm} s^{-1}_{mk}\right] s_{kj} \tag{38}$$

For small elongation one has $s_{il}\epsilon_{lm} s^{-1}_{mj} \simeq \epsilon_{ij} - 2\epsilon_{ik} Q_{kj}$. Identification with Eqs. 36 and 24 then yields the result. A more general result can be obtained for arbitrary magnitude of $\mathbf{Q}$.

in Eq. 32, assuming infinitesimal time steps, and pushing the corotational term to the left-hand-side, one obtains a coarse-grained version of the shear decomposition equation 30. There are two additional complications however in deriving this coarse-grained equation. First the averaging operators $\langle\cdot\rangle$, defined as in Eq. 19 but for triangles instead of cells, are applied over triangles with different areas in the tissue states I_n^1 and I_n^2. Second one would like to replace the corotational terms $\sim \langle\omega Q\rangle$ by $\langle\omega\rangle\langle Q\rangle$ in the definition of the corotational derivative, Eq. 29. These differences can be captured by introducing correcting terms to the coarse-grained version of Eq. 30. These correcting terms arise from correlations between deformations of the triangles and the triangle shapes, and are a consequence of the coarse-graining operation of going from the cellular scale to the tissue scale.

Overall, what we have gained is a rigorous method to calculate different contributions to tissue deformations.

4. Tissues as active fluids

Using the ideas introduced above, we now describe tissues as active fluids. "Active" systems are driven out of equilibrium by chemical reactions; typically through consumption of a fuel molecule (such as ATP in a cell) which is provided to the system to maintain it out of equilibrium. The hydrodynamic approach to describe an active system close to equilibrium uses an assumption of local equilibrium to identify a set of generalized forces and fluxes within the system. These generalized forces and fluxes are non-equilibrium properties and vanish at equilibrium. For instance, in a simple compressible active fluid, one can choose as generalized forces the non-equilibrium stress tensor σ_{ij} and the rate of fuel consumption r, and as conjugate generalized fluxes the shear rate v_{ij} and the chemical potential of the fuel reaction $\Delta\mu$. Once these forces and fluxes are recognized, non-equilibrium equations are obtained by expanding linearly the forces into fluxes:

$$\sigma_{ij} = \bar{\eta} v_{kk}\delta_{ij} + \eta\tilde{v}_{ij} + \zeta\Delta\mu\delta_{ij} \tag{40}$$

$$r = \zeta v_{kk} + \Lambda\Delta\mu \tag{41}$$

where $\bar{\eta}$, η, ζ, Λ are phenomenological coefficients which are constrained by Onsager symmetry relations. $\bar{\eta}$, η corresponding to the fluid bulk and shear viscosity, and $\zeta\Delta\mu$ is the active stress in the system, which is borne out by consumption of the fuel. These coefficients are not known a priori but can be measured experimentally, or could be derived from an analysis of the microscopic dynamics. The advantage of this formulation lies in its simplicity, the relatively small number of parameters that it introduces (compared to a full microscopic description of the system), and its generic aspect, as many systems with the same symmetries would be described by the same equations.

Even a non-deforming, steady-state tissue has ongoing cellular active processes which consume energy, such that the idea of expansion around the thermodynamic equilibrium, as described above, does not apply. However, in the approaches below one retains the idea of performing an expansion around steady-state, and retaining large-scale variables such as the stress tensor and shear flow in the physical description.

4.1. **Net cell division and homeostatic pressure.** In general one may expect that the rate of cell division and delamination in a tissue is sensitive to the cell density. The delamination rate k_a for instance, can arise at least in part from "crowding-induced delamination", an effect whereby cells whose area is becoming too small react, passively or actively, by extruding from the plane of the epithelium. Such effects can be introduced in a continuum theory of tissues by postulating a dependency of the net cell division rate, $k_d - k_a$, on the cell number density n:

$$k_d - k_a = -\kappa \frac{n - n_H}{n_H} \ . \tag{42}$$

As shown schematically below, such a relation implies that cell division occurs at low cell density, cell death or delamination occurs at high density, and a balance is reached at a particular equilibrium density n_H. The parameter κ is an inverse time scale which quantifies how strongly the tissue would react to a change in cell density by stimulating cell division or death. κ can be seen as a phenomenological parameter; and Eq. 42 as a linear expansion of the unknown rate of net cell division into the cell density. This approach is similar to the method for obtaining constitutive equations in close-to-equilibrium linear thermodynamics.

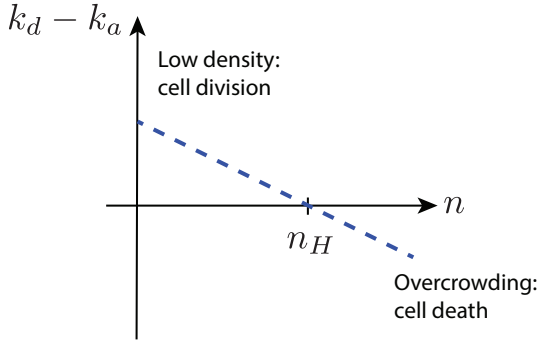

In parallel, one also expects that stresses in the tissue are sensitive to cell density. This can be captured by stating that the pressure in the tissue P (with P related to the trace of the stress tensor, $P = -\frac{1}{2}\sigma_{kk}$) is dependent on the tissue cell density:

$$P = P_H + \chi \frac{n - n_H}{n_H} \ , \tag{43}$$

where χ is here a bulk elastic modulus. This equation simply captures the fact that cells are likely to have a preferred area (or preferred volume in 3D), and deviations from this preferred area generates a pressure. In the relation above P_H is the pressure existing at the homeostatic point $n = n_H$ where cell death and cell extrusion balance each other.

Although Eq. 43 corresponds to an elastic behaviour on short time scales, the long-time-scale effect of a density-dependent net cell division rate is to fluidify the tissue. Intuitively, this is because putting the tissue under positive excess pressure relative to the homeostatic pressure, for instance, increases the cell death rate; reducing the area of the tissue. Subjected to this excess positive pressure, on long time scales the tissue will eventually

disappear completely. To see this, one can combine the cell number balance equation 25 with Eqs. 42 and 43 to obtain:

$$\frac{DP}{Dt} + \kappa \frac{n}{n_H}(P - P_h) = -\chi \frac{n}{n_H} \partial_k v_k \tag{44}$$

with $\frac{DP}{Dt} = \partial_t P + v_k \partial_k P$ is the convected time derivative of the pressure. For small variation of n around the reference density n_H, one recognizes the form of an equation describing a Maxwell fluid (see Eq. 4). By analogy one then sees that χ/κ plays the role of a viscosity, and $1/\kappa$ is the Maxwell viscoelastic timescale on which the system transitions from a solid to liquid behaviour.

4.2. **Tensor of cellular rearrangements and anisotropic stress.** We have introduced a tensor of cellular rearrangements R_{ij} in Eq. 30. We now would like to postulate a constitutive equation that would tell us how this tensor changes in time. Here we are guided by symmetry principles: the tensor of cellular rearrangement has the properties of a nematic, and so can be driven only by other nematic tensors. On this basis one can write

$$R_{ij} = \frac{1}{\tau} Q_{ij} + \lambda \left(p_i p_j - \frac{1}{2} \delta_{ij} \right) \ . \tag{45}$$

The first term on the right-hand side describes an effect of cell elongation on cellular rearrangements, occurring on a characteristic timescale τ. The second term describes the effect of cell planar polarity on cellular rearrangements. In some cases, as in germ band elongation in *Drosophila*, it is thought that cell planar polarity pathways leads to accumulation of force-generating myosin on cellular junctions with a specific orientation, triggering polarized cellular rearrangements. Such an effect is captured in the continuum theory by this second term, with λ an inverse time scale.

We have discussed in the previous section the tissue pressure, but in addition the full stress tensor of the tissue σ_{ij} has an anisotropic part $\tilde{\sigma}_{ij}$, such that

$$\sigma_{ij} = -P\delta_{ij} + \tilde{\sigma}_{ij} \ . \tag{46}$$

Note that we consider here the stress tensor to be symmetric. Here as well it is natural to assume that cells have a preferred elongation and that elastic restoring forces arise when cells elongate. In the absence of planar cell polarity, we expect that the preferred cell shape is isotropic, and so verifies $Q_{ij} = 0$. Then one can write the constitutive equation for the anisotropic part of the stress tensor:

$$\tilde{\sigma}_{ij} = 2\bar{K} Q_{ij} + \zeta \left(p_i p_j - \frac{1}{2} \delta_{ij} \right) \ , \tag{47}$$

where $\bar{K}$ is an elastic shear modulus, and ζ can be called an active anisotropic stress, in analogy with the hydrodynamic equations for an active fluid.

We first observe that, as was the case in section 4.1 with density-dependent cell division and death, here the dependency of topological transitions on cell elongation leads to fluidification of the tissue, with respect to pure shear. Indeed considering the case $\lambda = \zeta = 0$

for simplicity, one obtains combining Eqs. 30, 45 and 47:

$$\tilde{\sigma}_{ij} + \tau \frac{D\tilde{\sigma}_{ij}}{Dt} = 2\bar{K}\tau\tilde{v}_{ij} \ . \tag{48}$$

One recognizes the constitutive equation of a Maxwell viscoelastic fluid, with viscosity $\eta = \bar{K}\tau$ and Maxwell viscoelastic time scale τ. Here applying a stress to the tissue leads to cell elongation and a corresponding elastic restoring force, on short time scale. However the increase in cell elongation triggers topological rearrangements which relax the overall cell elongation. Therefore, to sustain a constant stress, the cells must elongate again, and the tissue as a whole keeps elongating and flows.

To discuss the effect of the contributions proportional to cell planar polarity, we now consider the deformation of a rectangular, uniform tissue, with polarity oriented along the vertical axis $\mathbf{p} = (0, 1)$. We have in mind a situation where junctional tension increases on vertical junctions in the tissue (red junctions in the schematic below), and so we expect $\zeta > 0$ (as there is a high σ_{yy} active stress compared to σ_{xx}) and $\lambda < 0$ (as removing vertical junctions should push cells away from each other along the horizontal direction, giving rise to a negative shear v_{yy} and positive shear v_{xx}). For $t < 0$ we assume that there is no cell elongation, $\mathbf{Q} = 0$, and $\lambda = \zeta = 0$. For $t \geq 0$ these last two parameters take non-zero values.

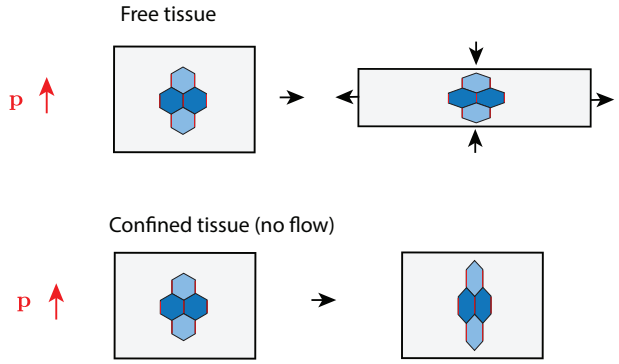

If the tissue is free to deform, there is no overall stress and $\tilde{\sigma}_{ij} = 0$, so that following the constitutive equation 47, the cell elongation instantaneously jumps to a non-zero value:

$$Q_{yy} = -Q_{xx} = -\frac{\zeta}{4\bar{K}}, Q_{xy} = 0 \ . \tag{49}$$

In practice, dissipative effects that have not been introduced here would determine the time scale on which the cell elongation relaxes to this steady-state value. We also see that with the signs discussed above, one has $Q_{xx} > 0$ and $Q_{yy} < 0$, and cells elongate along the horizontal direction. The anisotropic shear decomposition equation then implies that

$$\tilde{v}_{yy} = -\tilde{v}_{xx} = \frac{1}{2}\left(\lambda - \frac{\zeta}{2\tau\bar{K}}\right) \ , \tag{50}$$

where we have used that $\partial_t Q_{ij} = 0$ for $t > 0$. Because $\lambda < 0$ and $\zeta > 0$, there is a constant negative shear $\tilde{v}_{yy}$, so that the rectangular tissue is continuously deforming by expanding

along the x direction and constricting along the y direction, a mode of deformation that developmental biologists refer to as "convergence-extension". We find that both active cellular rearrangements and the active stress contribute to the overall tissue flow. Only the active stress however sets the value of cell elongation.

It is interesting to contrast this to the situation where the homogeneous rectangular tissue is confined and can not deform. In that case $\tilde{v}_{ij} = 0$ as there can not be a large-scale flow. The cell elongation dynamics is given by

$$\frac{dQ_{yy}}{dt} + \frac{1}{\tau} Q_{yy} = -\frac{\lambda}{2} \tag{51}$$

which leads to $Q_{yy} = -Q_{xx} = -\frac{\lambda\tau}{2}(1 - e^{-\frac{t}{\tau}})$. Here the cell elongation progressively builds up, through topological transitions, such that cells are eventually elongated along the y direction ($Q_{yy} > 0$ as $\lambda < 0$). Therefore, here one expects that cells have their longer junctions along the y direction, and per our initial assumptions, these vertical junctions also have higher line tension than their horizontal counterparts. The fact that longer junctions in the tissue have a higher line tension seems counterintuitive. Interestingly such a configuration is sometimes observed in biological tissues. The framework described here allows to rationalize this somewhat surprising behaviour.

5. Applications

In this section we will discuss simple examples, to see how to relate the concepts developed above to real biological systems.

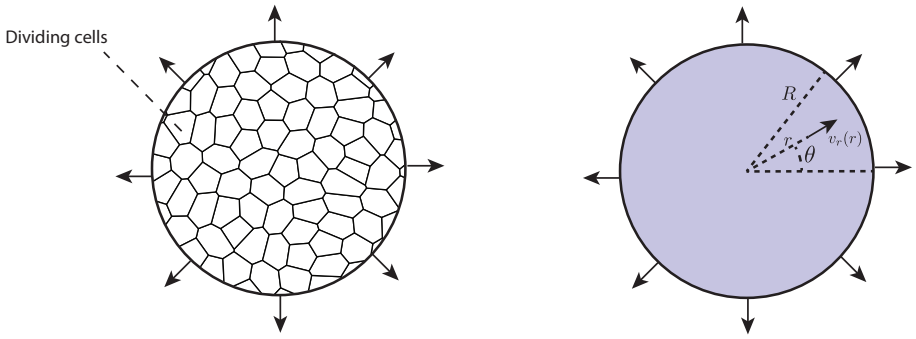

Figure 1. A growing circular tissue, with cells dividing with cell division rate k_d. The tissue flows with a radial velocity v_r.

5.1. **Growth of a circular tissue.** Here we consider a growing two-dimensional, circular, rotationally symmetric tissue with radius R. Cells flow in the tissue with a radial velocity field v_r and divide with a constant rate k_d. The cell number density in the tissue is denoted n. We use polar coordinates r, θ. The components of the symmetric gradient of flow are

$$v_{ij} = \begin{pmatrix} v_{rr} & v_{r\theta} \\ v_{\theta r} & v_{\theta\theta} \end{pmatrix} = \begin{pmatrix} \partial_r v_r & 0 \\ 0 & \frac{v_r}{r} \end{pmatrix} . \tag{52}$$

The stress tensor is assumed to be isotropic, such that the components of the stress tensor read

$$\sigma_{ij} = \begin{pmatrix} \sigma_{rr} & \sigma_{r\theta} \\ \sigma_{\theta r} & \sigma_{\theta\theta} \end{pmatrix} = \begin{pmatrix} -P & 0 \\ 0 & -P \end{pmatrix} , \tag{53}$$

with P the pressure in the tissue, given by

$$P = \chi \frac{n - n_H}{n_H} , \tag{54}$$

with n_H a constant and χ a tissue elastic modulus. The tissue is free to expand, and therefore has zero pressure at its boundary. The expression of radial force balance in polar coordinates is

$$\partial_r \sigma_{rr} + \frac{1}{r}\partial_\theta \sigma_{\theta r} + \frac{1}{r}(\sigma_{rr} - \sigma_{\theta\theta}) = 0 . \tag{55}$$

Here $\sigma_{rr} = -P$, $\sigma_{r\theta} = 0$, $\sigma_{\theta\theta} = -P$ and so

$$\partial_r P = 0 . \tag{56}$$

The pressure P is simply uniform, equal to 0 at the tissue boundary, so $P = 0$ and $n = n_H$. In other words, the tissue is free to assume its preferred cell density.

Using the fact that in polar coordinates, the divergence of a radial vector field $\mathbf{f} = f_r \mathbf{e}_r$ is given by $\partial_i f_i = \partial_r f_r + \frac{f_r}{r}$, the balance of cell number reads here

$$\partial_t n + \partial_r (n v_r) + \frac{n v_r}{r} = n k_d . \tag{57}$$

However we have seen that $n = n_H$, so the equation for the balance of cell number then reduces to $\partial_r v_r + \frac{v_r}{r} = k_d$. When the cell division rate k_d is uniform, the velocity profile reads, noting that the velocity v_r must vanish for $r = 0$:

$$v_r = \frac{k_d}{2} r . \tag{58}$$

The solution for the flow profile of a circular tissue growing without external constraint and without external forces is then a simple linear function of the radius.

In addition using that $\frac{dR}{dt} = v_r(R)$, one obtains $\frac{dR}{dt} = \frac{k_d}{2} R$ and so

$$R = R_0 e^{k_d t/2} , \tag{59}$$

i.e., the tissue undergoes exponential growth with characteristic timescale $2/k_d$.

5.2. **Application: expansion velocity of a confined proliferating tissue.** Here we discuss again a growing tissue, but in a different set-up. We consider a two-dimensional tissue which is proliferating with a free interface, along the direction x. The tissue extension goes to infinity for $x \to -\infty$. We denote n the cell number density in the tissue. The tissue flows along the x axis with velocity v_x.

The cell number density balance equation reads here

$$\partial_t n + \partial_x (n v_x) = (k_d - k_a) n , \tag{60}$$

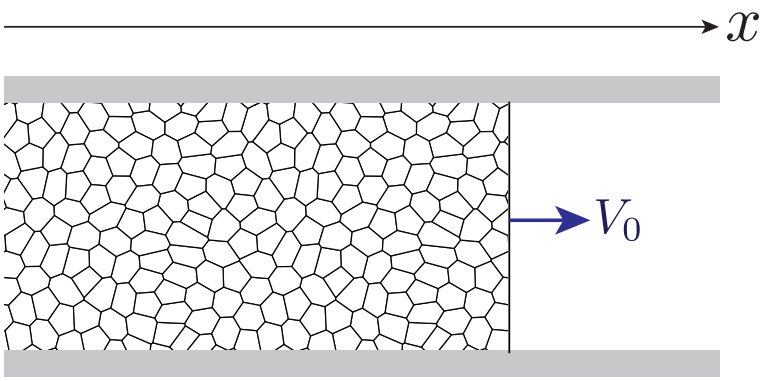

with $k_d - k_a$ the net cell division rate. As discussed in section 4.1, we assume here that proliferation is dependent on the cell density, such that the net cell division rate is

$$k_d - k_a = -\frac{1}{\tau}\frac{n - n_H}{n_H} \tag{61}$$

with τ a characteristic timescale for cell division. The constitutive equation for the stress in the tissue reads

$$\sigma_{xx} = -P_H - \chi\frac{n - n_H}{n_H} \tag{62}$$

where P_H is the proliferative pressure in the tissue, and χ is a bulk elastic modulus. The proliferative pressure is assumed to be uniform. Here we also assume that a friction force acts against the movement of the tissue, with friction coefficient ξ. The force balance equation in the tissue then reads

$$\partial_x \sigma_{xx} = \xi v_x \ . \tag{63}$$

For our calculations we restrict ourselves to small deviations away from the reference density n_H, such that $n = n_H + \delta n$, with $\delta n \ll n_H$. We obtain an equation for the cell density, to linear order in δn and in the velocity v_x, starting from the cell number balance equation and expanding in small δn, v_x:

$$\begin{aligned} \partial_t n + \partial_x(n v_x) &= -\frac{1}{\tau}\frac{n - n_H}{n_H} n \\ \partial_t(n_H + \delta n) + \partial_x((n_H + \delta n)v_x) &= -\frac{1}{\tau}\frac{\delta n}{n_H}(n_H + \delta n) \\ \partial_t \delta n + n_H \partial_x v_x &= -\frac{1}{\tau}\delta n \end{aligned} \tag{64}$$

where two non-linear terms have been removed in the last line. We now rewrite this last equation in the referential of the moving boundary, moving with constant velocity V_0. We introduce the variable relative to the moving interface, $z = x - V_0 t$. At steady-state, in the co-moving referential, $\partial_t \delta n \to -V_0 \partial_z \delta n$ and $\partial_x \to \partial_z$. One then obtains the steady-state

equation:

$$-V_0\partial_z\delta n + n_H(\partial_z v_x) = -\frac{1}{\tau}\delta n \ . \tag{65}$$

To make further progress we need to calculate the velocity v_z. The velocity field can be obtained by solving the force balance equation 63:

$$-\frac{\chi}{n_H}\partial_x\delta n = \xi v_x \tag{66}$$

and replacement in the cell number density equation then gives

$$-V_0\partial_z\delta n - \frac{\chi}{\xi}(\partial_z^2\delta n) = -\frac{1}{\tau}\delta n \ . \tag{67}$$

One now considers the case of a small expansion velocity V_0, such that the first term in the equation above can be neglected and the cell number density obeys the equation

$$-\frac{\chi}{\xi}\partial_z^2\delta n + \frac{1}{\tau}\delta n = 0 \ . \tag{68}$$

We will now use the fact that the stress at the boundary of the tissue $z = 0$ vanishes, and that the cell number density does not diverge for $z \to -\infty$, to solve for the cell number density and flow profile in the tissue. The solution is

$$\delta n = Ce^{z\sqrt{\frac{\xi}{\chi\tau}}} \tag{69}$$

with C a constant to determine. The stress is

$$\sigma_{xx} = -P_H - \chi\frac{C}{n_H}e^{z\sqrt{\frac{\xi}{\chi\tau}}} \ . \tag{70}$$

Since the tissue is free to expand at its boundary, $\sigma_{xx}(z = 0) = 0$, and $C = -P_H\frac{n_H}{\chi}$. The velocity is

$$\begin{aligned} v_x = \frac{\partial_z\sigma_{xx}}{\xi} = -\frac{\chi\partial_z\delta n}{\xi n_H} = \frac{P_H}{\xi}\sqrt{\frac{\xi}{\chi\tau}}e^{z\sqrt{\frac{\xi}{\chi\tau}}} \\ = P_H\frac{1}{\sqrt{\xi\chi\tau}}e^{z\sqrt{\frac{\xi}{\chi\tau}}} \ . \end{aligned} \tag{71}$$

The velocity of expansion of the tissue, V_0 reads

$$V_0 = v_x(z = 0) = P_H\frac{1}{\sqrt{\xi\chi\tau}}. \tag{72}$$

The speed of expansion of the tissue is slowed down by the friction coefficient acting against tissue motion, ξ, and by the tissue bulk elastic modulus χ. In this model all the tissue growth occurs in a boundary layer near the interface, with a size $\sqrt{\chi\tau/\xi}$. This boundary layer arises because of the non-zero friction coefficient ξ. Further away from the interface, the pressure relaxes to the homeostatic pressure and there is no net cell division.

5.3. **Application: laser ablation experiment.**

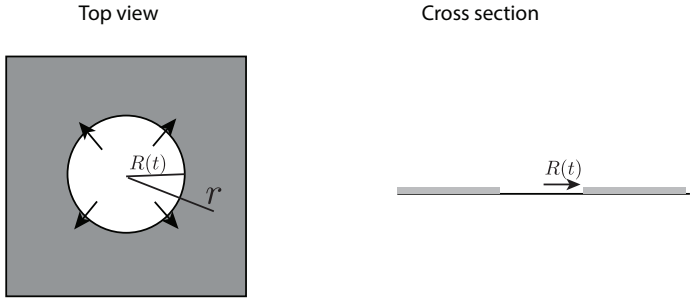

We consider here the process of the opening of a hole by laser ablation of an epithelial tissue. This experimental technique is used to quantify stresses in the tissue, by using the opening velocity of the hole as an indirect measurement of the state of stress of the epithelium. Because this technique does not directly measure a force, it can not be used to measure actual stresses or tensions, but can be used to measure relative stresses or tensions at different places of the tissue, under the hypothesis that the viscosity or friction do not change significantly.

To treat this situation, we consider a circular hole made in an effectively infinite epithelium, which is assumed here to move without friction. The stress in the epithelium drives the expansion of the fluid around the hole. The radius of the hole changes over time and is given by the function $R(t)$. There is a symmetry of rotation such that in polar coordinates (r, θ), all quantities depend on r only. The total stress is taken to be equal to the sum of an elastic isotropic stress and a deviatoric viscous stress proportional to $\tilde{v}_{ij}$:

$$\sigma_{ij} = \left(\sigma_0 - \chi \frac{n - n_0}{n_0}\right) \delta_{ij} + 2\eta \tilde{v}_{ij} \tag{73}$$

where σ_0 and n_0 are the stress and cell density before laser ablation, χ the bulk tissue elastic modulus, and η the tissue shear viscosity. The cell density changes over time according to the cell number balance equation 25, with no division and delamination.

The force balance for the components of the stress in polar coordinates, σ_{rr} and $\sigma_{\theta\theta}$ ($\sigma_{r\theta} = 0$ with rotational symmetry), reads

$$\partial_r \sigma_{rr} + \frac{1}{r}(\sigma_{rr} - \sigma_{\theta\theta}) = 0 \ . \tag{74}$$

Using the constitutive relation and force balance equation, we look for an equation for the velocity field. From the constitutive equations we have:

$$(\sigma_{rr} - \sigma_{\theta\theta}) = 2\eta(\tilde{v}_{rr} - \tilde{v}_{\theta\theta}) = 2\eta \left(\partial_r v_r - \frac{v_r}{r}\right), \tag{75}$$

$$\partial_r \sigma_{rr} = -\chi \partial_r \frac{n}{n_0} + 2\eta(\partial_r \tilde{v}_{rr}) = -\chi \partial_r \frac{n}{n_0} + \eta \partial_r \left(\partial_r v_r - \frac{v_r}{r}\right) \ . \tag{76}$$

Plugging into force balance gives

$$-\chi \partial_r \frac{n}{n_0} + \eta \left(\partial_r^2 v_r + \frac{\partial_r v_r}{r} - \frac{v_r}{r^2}\right) = 0. \tag{77}$$

We now make the ansatz that the cell density does not change during the expansion of the hole, $n = n_0$. Solving the differential equation above, we then find:

$$v_r(r) = C_1 r + \frac{C_2}{r}. \tag{78}$$

We then impose the boundary conditions at infinity ($v_r(r) \to 0$ when $r \to \infty$) and at the edge of the hole ($\sigma_{rr}(R) = 0$)). The first boundary condition imposes $C_1 = 0$. This also implies that $\partial_r v_r + \frac{v_r}{r} = 0$, and so the cell number balance equation 25 reads:

$$\partial_t n + v_r \partial_r n + n\left(\partial_r v_r + \frac{v_r}{r}\right) = 0 \tag{79}$$

and since $\partial_r v_r + \frac{v_r}{r} = 0$, $n = n_0$ is indeed a solution of the equation above, so that the ansatz was justified.

The stress at the edge of the hole reads

$$\sigma_{rr}(R) = \sigma_0 + \eta\left(\partial_r v_r(R) - \frac{v_r(R)}{R}\right) \tag{80}$$

Plugging in the solution and setting $\sigma_{rr}(R) = 0$, we have $C_2 = \frac{\sigma_0}{2\eta} R^2$, such that the velocity field is given by:

$$v_r(r) = \frac{\sigma_0}{2\eta}\frac{R^2}{r} \ . \tag{81}$$

The dynamic equation for the hole radius is then

$$\frac{dR}{dt} = v_r(R) = \frac{\sigma_0}{2\eta} R, \tag{82}$$

with an exponentially increasing solution

$$R(t) = R(0) e^{\frac{\sigma_0}{2\eta} t}. \tag{83}$$

The initial velocity, which is often used to compare different states of stress in the tissue, is $v_0 = \frac{\sigma_0 R_0}{2\eta}$ with R_0 the initial radius of the hole. This velocity is indeed proportional to σ_0.

The equation above also predicts an exponential, accelerating expansion of the hole, with a time constant of expansion $\tau = \frac{2\eta}{\sigma_0}$ which is set by the initial stress in the tissue and the viscosity. This result is a consequence of our initial assumption that the tissue is fluid with respect to pure shear deformation, and is clearly unrealistic for the response of an epithelium over minutes when topological transitions do not have time to occur. In practice the model above could be considered as a short time-scale limit of a Kelvin-Voigt description of the tissue, with η the short time scale tissue viscosity. A more realistic description would also take into account the tissue elastic response to changes in cell elongation.

5.4. **Application: spontaneous flow in a confined epithelium.** Here we discuss a spontaneous flow instability which has been observed in tissues cultured *in vitro* in a confined environment.

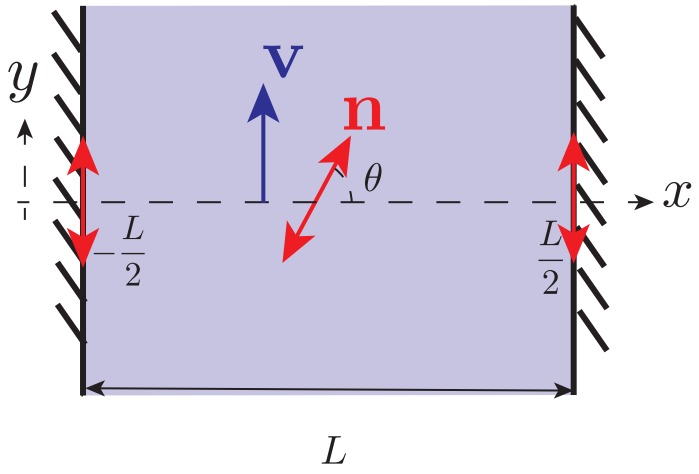

We consider a two-dimensional epithelium confined between two plates separated by a distance L along the x direction. We assume invariance by translation along the y direction. The epithelium has a cell elongation field $\mathbf{n} = (\cos\theta, \sin\theta)$ and velocity vector $\mathbf{v}$. The tissue is assumed to have a planar anchoring condition on the two confining plates, such that $\theta\left(-\frac{L}{2}\right) = \theta\left(\frac{L}{2}\right) = \frac{\pi}{2}$, and it is free to slide along the plates, such that $\sigma_{xy}\left(-\frac{L}{2}\right) = \sigma_{xy}\left(\frac{L}{2}\right) = 0$.

We assume that the stress tensor and dynamics of polarity field for the active fluid are given by

$$\sigma_{ij} = -P\delta_{ij} + 2\eta\tilde{v}_{ij} + \zeta\left[n_i n_j - \frac{1}{2}\delta_{ij}\right] + \frac{\nu}{2}(n_i h_j + n_j h_i - \frac{1}{2}n_k h_k \delta_{ij}) - \frac{1}{2}(n_i h_j - n_j h_i) \tag{84}$$

$$\frac{Dn_i}{Dt} = \frac{1}{\gamma}h_i - \nu\tilde{v}_{ij}n_j \ , \tag{85}$$

where $h_i = -\frac{\delta F}{\delta n_i}$ is the molecular field, with F the effective free energy, and we have used the corotational derivative

$$\frac{Dn_i}{Dt} = \partial_t n_i + v_j\partial_j n_i + \omega_{ij}n_j \ , \tag{86}$$

with $\omega_{ij} = \frac{1}{2}(\partial_i v_j - \partial_j v_i)$ the vorticity tensor. The tissue is assumed here to be incompressible, such that

$$\partial_i v_i = 0 \ . \tag{87}$$

The pressure P in Eq. 84 is a Lagrange multiplier enforcing incompressibility. The term proportional to ζ is an active anisotropic stress in the tissue. The terms proportional to $\mathbf{h}$ are stresses that arise from distorsion in the elongation field. The coefficient ν appears

both in the equation for the stress Eq. 84 and the equation for the polarity Eq. 85 as the model is inspired from close-to-equilibrium thermodynamics, for which Onsager symmetry relations imply the equality of these coefficients. Here we keep these coefficients equal for simplicity.

We assume that the free energy associated to the order parameter reads

$$F = \int_S dS \left[\frac{K}{2} (\partial_i \mathbf{n})^2 + \frac{\lambda}{2} (\mathbf{n}^2 - 1) \right] \tag{88}$$

with λ a Lagrange multiplier enforcing that the norm of the order parameter stays equal to 1. The molecular field reads:

$$h_i = K \Delta n_i - \lambda n_i \tag{89}$$

which can be rewritten

$$h_x = -\left[K(\partial_x \theta)^2 + \lambda \right] \cos\theta - K(\partial_x^2 \theta) \sin\theta \tag{90}$$

$$h_y = -\left[K(\partial_x \theta)^2 + \lambda \right] \sin\theta + K(\partial_x^2 \theta) \cos\theta \tag{91}$$

and as a result, denoting $h_{||} = n_x h_x + n_y h_y$ and $h_\perp = n_y h_x - n_x h_y$ the components of $\mathbf{h}$ parallel and perpendicular to $\mathbf{n}$,

$$h_{||} = -\left[K(\partial_x \theta)^2 + \lambda \right] \tag{92}$$

$$h_\perp = -K(\partial_x^2 \theta) \ . \tag{93}$$

At equilibrium, in the absence of flow, $\mathbf{h} = 0$. Taking into account the boundary conditions, the corresponding equation is solved by the uniform cell elongation axis $\theta = \frac{\pi}{2}$.

We now are going to determine whether this solution is stable. If the solution is unstable, a distorsion in the cell elongation pattern and a spontaneous flow can emerge in the system. To test this, we consider a perturbation around the equilibrium solution $\theta = \frac{\pi}{2} + \delta\theta$, with $\delta\theta \ll 1$. The incompressibility condition implies $\partial_x v_x = 0$, and v_x vanishes at the walls, hence $v_x = 0$.

The polarity dynamics equation gives

$$\partial_t n_x + \frac{1}{2}(\partial_x v_y) n_y = \frac{1}{\gamma} h_x - \frac{\nu}{2} (\partial_x v_y) n_y \tag{94}$$

$$\partial_t n_y - \frac{1}{2}(\partial_x v_y) n_x = \frac{1}{\gamma} h_y - \frac{\nu}{2} (\partial_x v_y) n_x \tag{95}$$

where we have used $\omega_{xy} = \frac{1}{2}\partial_x v_y$ and $\omega_{yx} = -\frac{1}{2}\partial_x v_y$. These relations can be rewritten using the identity $\partial_t \theta = n_x(\partial_t n_y) - n_y(\partial_t n_x)$ and Eq. 93:

$$\partial_t \theta = \frac{K}{\gamma} \partial_x^2 \theta - \frac{\partial_x v_y}{2} (-1 + \nu \cos 2\theta) \tag{96}$$

In the limit $\delta\theta \ll 1$, this becomes:

$$\partial_t \delta\theta \simeq \frac{K}{\gamma} \partial_x^2 \delta\theta + \partial_x v_y \frac{1+\nu}{2} \ . \tag{97}$$

We now need to determine the solution for the flow profile v_y. For this writing the force balance equations, taking into account the invariance with respect to y, one obtains:

$$\begin{aligned} \partial_x \sigma_{xx} &= 0 \\ \partial_x \sigma_{xy} &= 0 \ . \end{aligned} \tag{98}$$

The force balance relation implies that $\partial_x \sigma_{xy} = 0$, and σ_{xy} vanishes at the walls, hence $\sigma_{xy} = 0$. Using the constitutive equation for the stress 84, this condition gives:

$$\eta \partial_x v_y + \nu \cos\theta \sin\theta h_{||} + \frac{\nu}{2}(\sin^2\theta - \cos^2\theta) h_\perp + \frac{1}{2} h_\perp + \zeta \cos\theta \sin\theta = 0 \tag{99}$$

where one has used

$$\begin{aligned} n_x h_y + n_y h_x &= \cos\theta(h_{||}\sin\theta - h_\perp \cos\theta) + \sin\theta(h_{||}\cos\theta + h_\perp \sin\theta) \\ &= 2h_{||}\cos\theta\sin\theta + (\sin^2\theta - \cos^2\theta) h_\perp \end{aligned} \tag{100}$$

Besides, because $|\mathbf{n}| = 1$,

$$0 = n_x(\partial_t n_x) + n_y(\partial_t n_y) = \frac{1}{\gamma} h_{||} - \nu(\partial_x v_y) n_x n_y \ . \tag{101}$$

and therefore:

$$h_{||} = \nu\gamma(\partial_x v_y) n_x n_y \ . \tag{102}$$

Using then the expression for $h_{||}$ and $h_\perp$, Eq. 99 can be rewritten:

$$(\eta + \nu^2 \gamma \cos^2\theta \sin^2\theta)\partial_x v_y - \frac{K}{2}\partial_x^2\theta(1 - \nu\cos 2\theta) + \zeta\cos\theta\sin\theta = 0 \ . \tag{103}$$

which becomes in the limit $\delta\theta \ll 1$,

$$\partial_x v_y = \frac{K}{2\eta}(1+\nu)\partial_x^2 \delta\theta + \frac{\zeta}{\eta}\delta\theta \ . \tag{104}$$

Combining Eqs. 97 and 104, we can now obtain a differential equation for the orientation angular field $\delta\theta$:

$$\partial_t \delta\theta \simeq K\left(\frac{1}{\gamma} + \frac{(1+\nu)^2}{4\eta}\right)\partial_x^2\delta\theta + \frac{\zeta(1+\nu)}{2\eta}\delta\theta. \tag{105}$$

To find solutions for this equation, we use the ansatz $\delta\theta = \epsilon(t)\cos(\frac{\pi x}{L})$, which then gives:

$$\partial_t \epsilon \simeq \left[\frac{\zeta(1+\nu)}{2\eta} - K\left(\frac{1}{\gamma} + \frac{(1+\nu)^2}{4\eta}\right)\frac{\pi^2}{L^2}\right]\epsilon \tag{106}$$

The equation above exhibits an instability (exponentially growing solution) when

$$\frac{\zeta(1+\nu)}{2\eta K} > \left(\frac{1}{\gamma} + \frac{(1+\nu)^2}{4\eta}\right)\frac{\pi^2}{L^2} \tag{107}$$

or for the critical length

$$L > \pi\sqrt{\frac{K}{\zeta}}\sqrt{\frac{2\eta}{\gamma(1+\nu)}+\frac{1+\nu}{2}}\,. \tag{108}$$

An instability giving rise to a distorsion pattern and a spontaneous flow occurs for a contractile system, $\zeta > 0$, and for large enough confinement length. Indeed if the length of the tissue stripe is too small, distorsion patterns are too energetically costly and the instability can not arise.

Below is a sketch of the flow and cell elongation profile that grow beyond the instability threshold. Similar orientation and flow profiles are indeed observed experimentally by confining for instance RPE1 cells *in vitro*.

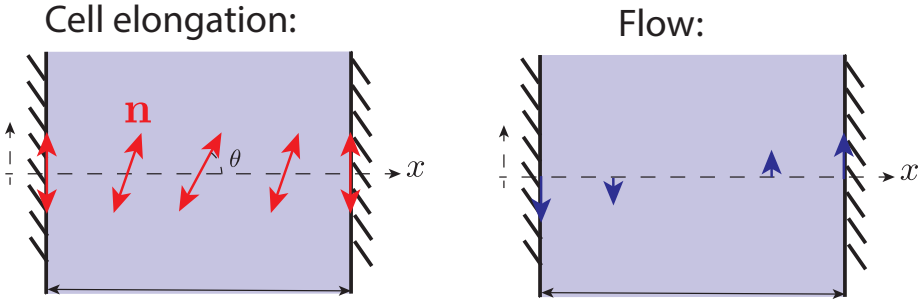

6. Concluding words

The physics of tissues at large scales has an extremely rich behaviour, as illustrated by some examples we have covered here. Additional examples can be found in the (non-exhaustive) list of references below. Large-scale tissue collective flows and deformations is also an active current area of research. In addition, during development, tissues form patterns of gene expression and signalling activity, an aspect that we have not discussed here.

References

[1] Pierre Recho, Jonas Ranft, and Philippe Marcq. One-dimensional collective migration of a proliferating cell monolayer. *Soft matter*, 12(8):2381–2391, 2016.

[2] John J Williamson and Guillaume Salbreux. Stability and roughness of interfaces in mechanically regulated tissues. *Physical review letters*, 121(23):238102, 2018.

[3] R Voituriez, Jean-François Joanny, and Jacques Prost. Spontaneous flow transition in active polar gels. *EPL (Europhysics Letters)*, 70(3):404, 2005.

[4] Karsten Kruse, Jean-Francois Joanny, Frank Jülicher, Jacques Prost, and Ken Sekimoto. Generic theory of active polar gels: a paradigm for cytoskeletal dynamics. *The European Physical Journal E*, 16(1):5–16, 2005.

[5] Pierre-Gilles De Gennes and Jacques Prost. *The physics of liquid crystals*, volume 83. Oxford university press, 1993.

[6] Philipp Khuc Trong, Ernesto M Nicola, Nathan W Goehring, K Vijay Kumar, and Stephan W Grill. Parameter-space topology of models for cell polarity. *New Journal of Physics*, 16(6):065009, 2014.

[7] Nathan W Goehring, Philipp Khuc Trong, Justin S Bois, Debanjan Chowdhury, Ernesto M Nicola, Anthony A Hyman, and Stephan W Grill. Polarization of par proteins by advective triggering of a pattern-forming system. *Science*, 334(6059):1137–1141, 2011.

[8] Boris Guirao, Stephane U Rigaud, Floris Bosveld, Anais Bailles, Jesus Lopez-Gay, Shuji Ishihara, Kaoru Sugimura, Francois Graner, and Yohanns Bellaiche. Unified quantitative characterization of epithelial tissue development. *Elife*, 4:e08519, 2015.

[9] Isabelle Bonnet, Philippe Marcq, Floris Bosveld, Luc Fetler, Yohanns Bellaïche, and François Graner. Mechanical state, material properties and continuous description of an epithelial tissue. *Journal of The Royal Society Interface*, 9(75):2614–2623, 2012.

[10] Guillaume Duclos, Christoph Erlenkämper, Jean-François Joanny, and Pascal Silberzan. Topological defects in confined populations of spindle-shaped cells. *Nature Physics*, 13(1):58, 2017.

[11] Matthias Merkel, Raphaël Etournay, Marko Popović, Guillaume Salbreux, Suzanne Eaton, and Frank Jülicher. Triangles bridge the scales: quantifying cellular contributions to tissue deformation. *Physical Review E*, 95(3):032401, 2017.

[12] Marko Popović, Amitabha Nandi, Matthias Merkel, Raphaël Etournay, Suzanne Eaton, Frank Jülicher, and Guillaume Salbreux. Active dynamics of tissue shear flow. *New Journal of Physics*, 19(3):033006, 2017.

[13] Raphaël Etournay, Marko Popović, Matthias Merkel, Amitabha Nandi, Corinna Blasse, Benoît Aigouy, Holger Brandl, Gene Myers, Guillaume Salbreux, Frank Jülicher, et al. Interplay of cell dynamics and epithelial tension during morphogenesis of the drosophila pupal wing. *Elife*, 4:e07090, 2015.

[14] Benoît Aigouy, Reza Farhadifar, Douglas B Staple, Andreas Sagner, Jens-Christian Röper, Frank Jülicher, and Suzanne Eaton. Cell flow reorients the axis of planar polarity in the wing epithelium of drosophila. *Cell*, 142(5):773–786, 2010.